Magnetic inhomogeneity in a multiferroic EuTiO_{3} thin film

Yanan Geng, J. H. Lee, D. G. Schlom, J. W. Freeland, and Weida Wu

Phys. Rev. B **87**, 121109 — Published 18 March 2013

DOI: 10.1103/PhysRevB.87.121109

Magnetic inhomogeneity in a multiferroic $EuTiO_3$ thin film

Yanan Geng[1], J.H. Lee[2], D.G. Schlom[3], J.W. Freeland[2], and Weida Wu[1*]

[1]*Department of Physics & Astronomy and Rutgers Center for emergent materials, Rutgers University, Piscataway, NJ 08854 USA*

[2]*Advanced Photon Source, Argonne National Laboratory, Argonne, IL USA*

[3]*Department of Material Science, Cornell University, Ithaca, NY USA*

We report on variable temperature magnetic force microscopy studies of a strain-enabled multiferroic $EuTiO_3$ film epitaxially grown on (110)-oriented $DyScO_3$ substrate. Our temperature and magnetic field-dependent studies clearly reveal an inhomogeneous magnetic state with coexistence of ferromagnetic and non-ferromagnetic states at low magnetic fields，which provides a microscopic origin of the anomalous missing moment in previous studies [J. H. Lee, et al, *Nature* 466, 19 (2010)]. The spins of the non-ferromagnetic phase can be aligned by modest magnetic fields (>1.5 T). The observed magnetic inhomogeneity probably originates from the coexistence of nearly degenerate magnetic ground states.

Multiferroics are materials which simultaneously exhibit electric and magnetic order.[1] Great interest has been generated in multiferroics because of the potential cross-coupling between the two order parameters, i.e. electric field controllable magnetic state and vice versa, which makes it promising in energy efficient memory devices and sensors applications.[2-4] Because of the scarcity of ferroelectricity and ferromagnetism in bulk single-phase multiferroics,[5] much attention has been focused on complex thin-film heterostructures between ferroelectric and magnetostrictive materials to realize effective magnetoelectric coupling by harnessing interfacial strain.[4]

In fact, interfacial strain has been demonstrated as an effective method to tailor the physical properties of thin films,[6-10] including controlling magnetic and electric properties in thin film multiferroics.[4, 6, 11] Furthermore, epitaxial strain might even induce emergent ground states which are absent in the bulk materials.[9, 12] E.g., $EuTiO_3$ thin films that were epitaxially

grown on $DyScO_3$ by Lee et al. became ferroelectric (FE) (T_{FE}=250 K) and ferromagnetic (FM) (T_C=4.5 K).[12] This strain-induced multiferroicity in $EuTiO_3$ was initially proposed by Fennie and Rabe using first principle calculations, where they showed that the ground state of $EuTiO_3$ can be tuned into a ferroelectric-ferromagnet by applying sufficient biaxial lattice strain.[12, 13] The theoretical prediction was inspired by the observation of strong spin-phonon coupling in bulk $EuTiO_3$ in the earlier experimental studies by Katsfuji and Takagi.[14] Recent experimental consensus about the ground state of bulk $EuTiO_3$ is that the crystal symmetry (*I*4/*mcm*) was lower than that in previous reports (*Pm*3*m*) due to complex oxygen octahedral tilts.[15-18] Consistently, first-principle calculations not only confirmed these new experimental results, but also pointed to a whole family of nanoscale twinned phases with nearly degenerate energies, which provides a theoretical basis for phase coexistence in the $EuTiO_3$ system.[12, 19-21]

Though the strain-induced multiferroicity has been confirmed experimentally, the saturation magnetization (~ $3\mu_B$ / Eu^{2+}) of the $EuTiO_3$ thin films is significantly smaller than the expected value (~7 μ_B / Eu^{2+}).[12] One possible scenario to resolve the missing moment mystery is a non-uniform magnetic state where the FM and non-FM phases coexist. However, there is no microscopic evidence for the magnetic inhomogeneity. Herein, we report variable temperature magnetic force microscopy (VT-MFM) studies on a specimen of $EuTiO_3$/$DyScO_3$ (ETO/DSO) from the same batch as those examined in Ref. 12. Besides confirming the ferromagnetic phase transition at 4.3 K, our MFM results provide direct evidence of magnetic inhomogeneity of coexisting FM and possibly paramagnetic phases, a microscopic explanation of the missing moment mystery in previous studies.[12]

A 22-nm-thick epitaxial $EuTiO_3$ film was grown on (110)-oriented single crystalline $DyScO_3$ substrate using molecular beam epitaxy method.[6] $DyScO_3$ has an orthorhombic unit cell with a = 5.440 Å, b = 5.717 Å, c = 7.903 Å at room temperature, which is often referred as pseudo-cubic with lattice constant about 3.944 Å.[22-24] Thus, the epitaxial $EuTiO_3$ film has a biaxial tensile strain of +1.1% as confirmed by spatially averages x-ray diffraction. The MFM experiments were performed in a homebuilt atomic force microscope using piezoresistive cantilever ($k \approx 3$ N/m, $f_0 \approx 35$ kHz), which is interfaced with a Nanoscope IIIa controller (Bruker).[8, 25] MFM tips were prepared by coating bare tips with nominally 60 nm Co thin film

using e-beam evaporation. MFM images were taken in a linear mode, in which the topography and lift scan lines are interleaved; the lift height was ~40 nm. The MFM signal, the shift of the cantilever's resonant frequency, is approximately proportional to the stray field gradient ($\partial_z^2 B_z$).[26-28] Magnetization measurements were performed in a superconducting quantum interference device magnetometer (SQUID).

Magnetization measurements of ETO/DSO films are non-trivial because the large paramagnetic response from the thick $DyScO_3$ substrate dominates the total magnetic signal in high applied magnetic fields.[29] The susceptibility anomaly of the antiferromagnetic (AFM) transition at T_N=3.1 K of $DyScO_3$ would interfere with the magnetization measurement even in low magnetic fields.[12] Since the MFM signal is only sensitive to stray field gradients, there is no magnetic contrast above a uniformly magnetized magnet with a flat surface.[25] Therefore, the MFM technique is insensitive to the magnetic response from $DyScO_3$ substrate, in either the paramagnetic or the AFM phase, i.e., MFM is an ideal tool to explore the local magnetic property of the epitaxial $EuTiO_3$ film.

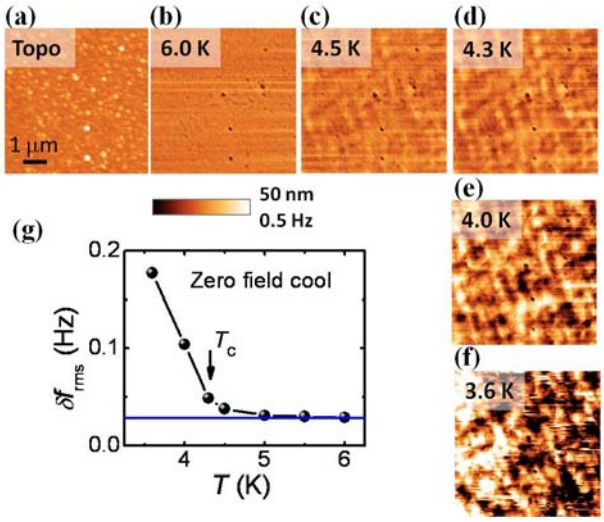

FIG.1. (Color online) Topographic (**a**) and MFM [(**b**)-(**f**)] images (size: 6 × 6 μm^2) were taken at the same location with zero magnetic field after ZFC. The color scale range is 50 nm (0.5 Hz) for topography (MFM) image. (g) Temperature dependence of the RMS values of MFM images. The blue line indicates the background of RMS values (above T_C).

Figure 1 shows the topographic image and temperature-dependent MFM images of the ETO/DSO film after zero field cooling (ZFC). As shown in Fig. 1(b), no MFM contrast is

observed above 4.5 K, except a few dark spots due to electrostatic interaction of topographic features. Below 4.5 K, non-uniform magnetic contrast emerges and gets stronger as temperature is lowered, indicating the appearance of magnetic order moments below the FM phase transition. To quantify the observed magnetic behavior of ETO/DSO, the temperature dependence of the root mean square (RMS) values of MFM images was plotted in Fig. 1(g). The RMS value of a MFM image is defined as $\delta f_{RMS} = \sqrt{\sum (f_i - f_0)^2 / (N-1)}$, where f_i is the MFM signal at each pixel, f_0 is the average value of the MFM signal, and N is the total number of pixels of the image. The RMS value is a statistical measure of the deviation of magnetic signal from its mean value, i.e. the contrast of a MFM image, assuming that the characteristic length of magnetic features is much smaller that the size of the MFM image. The sharp rise of the RMS value at 4.3 K indicates the formation of multi-domain state which enhances the deviation of the MFM signal from its mean value, confirming the FM phase transition in this tensile-strained $EuTiO_3$ film.[12]

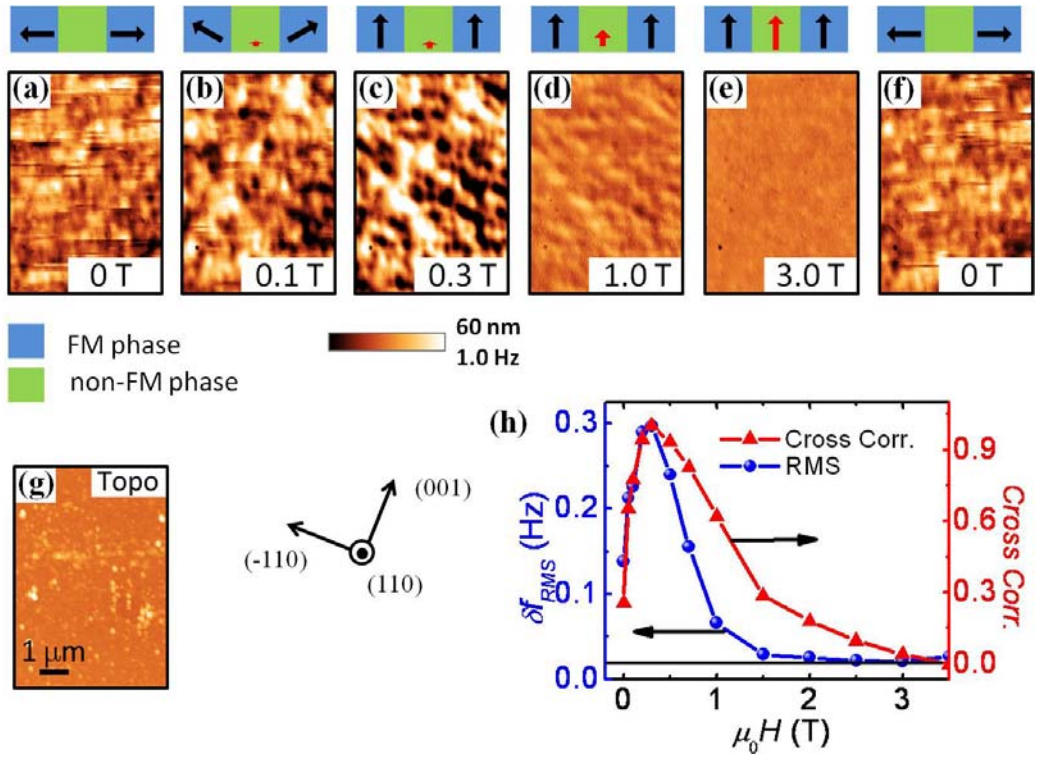

FIG. 2. (Color online) Magnetic field dependent MFM [(**a**)-(**f**)] and topographic (**g**) images were taken at the same location at 3.2 K after ZFC. The cartoons above MFM images represent the magnetic moments under various applied magnetic fields. (**f**) was measured at

zero field after application of magnetic fields (5 T). (**h**) Magnetic field dependence of the RMS value (blue) of the MFM images at 3.2 K and the cross correlation coefficient (red) between the 0.3 T MFM image (**c**) and all the MFM images. The inset between (**g**) and (**h**) shows the crystallographic orientations of the sample relative to scan images.

Previous x-ray magnetic circular dichroism (XMCD) studies confirmed that each Eu^{2+} in the ETO/DSO film carries the expected moment of 7 μ_B under high magnetic fields at $T>T_C$.[12, 30] However, the magnetization measurement indicated that the saturation moment in low field at the zero temperature limit is lower (~3 μ_B/Eu^{2+}), [12] indicating the possibility of an inhomogeneous magnetic ground state, e.g. a mixture of FM phase and non-FM phase [likely paramagnetic (PM) phases]. To test this hypothesis, we carried out MFM measurements at various magnetic fields at 3.2 K after ZFC. Fig. 2(a)-2(f) show a set of MFM images (size: 7.4×5 μm^2) at a different location from that in fig.1. From 0 T to approximately 0.25-0.3 T, the MFM contrast gets stronger at higher magnetic fields, and the magnetic patterns change a lot. On the other hand, the MFM contrast decreases sharply at magnetic fields from 0.3 T to 1.5 T, while the magnetic pattern is relatively static. As shown in fig. 3(e), the magnetic patterns disappear at fields above 1.5 T, indicating a saturated magnetic state with a uniform magnetization consistent with the high-field XMCD. The intriguing field-dependent behavior of locally inhomogeneous magnetic regions is summarized by the RMS values of MFM images, the blue spheres in Fig. 2(h), and by the cross correlation coefficients between the 0.3 T image and the others, the red triangles in Fig. 2(h).

Based on the magnetic field dependence of RMS values and cross correlation coefficients, several points can be drawn from our MFM data. First, the in-plane magnetic domains and the inhomogeneous magnetic state at low fields (0-0.3 T) produces a complicated MFM pattern. Note that the film has an in-plane easy axis due to the biaxial tensile strain.[31] The MFM images at zero field show a switching behavior, namely sudden change of MFM signal between adjacent scan lines in Fig. 2(a), i.e. horizontal line features. These horizontal lines indicate sudden changes of in-plane moments in the FM domains, probably due to the proximity of a significant stray field from MFM tip that is larger than the local coercive field. The spins of the FM part are gradually tilted out-of-plane (OOP) by the external magnetic

field, while the induced moment from non-FM phase is negligible at low fields ($\mu_0 H$<0.3 T). Thus, the RMS values and the cross-correlation coefficients of MFM images increased gradually. The moments of the FM part were practically aligned with external magnetic field at approximately 0.25–0.3 T. Consistently, the MFM pattern is hysteretic at low fields ($\mu_0 H$<0.3 T), e.g. the difference between Fig. 2(a) and Fig. 2(f), before and after application of high magnetic fields. The hysteresis at low fields is in good agreement with formation of magnetic domains. Second, at intermediate fields (0.3<$\mu_0 H$<1.5 T), the induced magnetization of the non-FM parts increased slowly while that of the FM parts were already in the saturated state (i.e. unchanged). As a result, the MFM contrast (i.e. the RMS value) decreases with increasing magnetic fields, while the magnetic pattern changes gradually, as indicated by the slower decrease of positive cross-correlations between MFM images at this intermediate field range. Consistently, the magnetic patterns were reversible, i.e. independent of the magnetic field sweeping direction at fields above 0.3 T. Third, at higher fields (>1.5 T), the magnetic pattern disappeared except a few spots probably due to defects, and the RMS values (due to noise) of MFM images are essentially constant, suggesting that the $EuTiO_3$ film was in the saturated state. In other words, the magnetic inhomogeneity can be suppressed by modest magnetic fields (>1.5 T). Previous XMCD studies suggested that 5 T magnetic field is strong enough to align all Eu^{2+} moments at $T>T_C$, in good agreement with our MFM observation of lower saturation field (~1.5 T) at $T<T_C$.[12, 14] The evolutions of FM and non-FM moments with applied magnetic fields are qualitatively summarized in the cartoons above each MFM image.

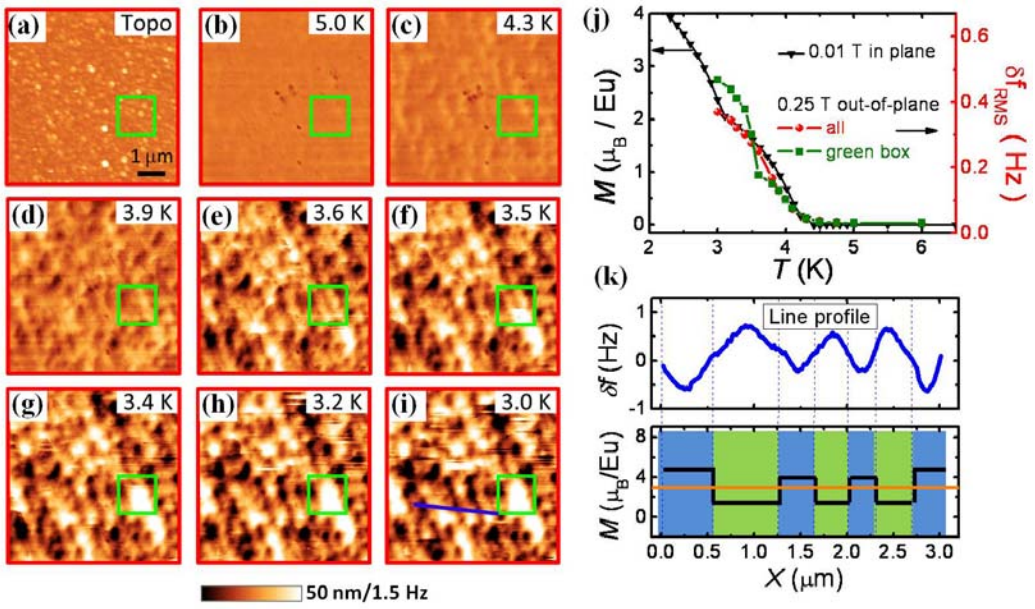

FIG. 3. (Color online) (**a**)-(**i**), the topographic (**a**) and temperature-dependent MFM [(**b**)-(**i**)] images taken under 0.25 T out-of-plane external field. The scan size is 6 × 6 μm^2, with color scale 50 nm (1.5 Hz) for topography (MFM). Green boxes mark the same location in different images. (**j**), the temperature dependence of the magnetization of ETO/DSO at 0.01 T in-plane field (black curve), the temperature dependence of the RMS values were calculated from the whole MFM image (red) and green box area (green), respectively. (**k**), a representative line cut on MFM image at 3.0 K along the blue line (upper panel) and a schematic illustration of the magnetization (lower panel) along the line profile. Blue (green) color represents FM (non-FM) phase in the film.

To shed some light on the nature of the magnetic inhomogeneity, we performed temperature-dependent MFM studies with a 0.25 T OOP magnetic field, which is strong enough to align the in-plane FM domains but not enough to saturate the non-FM moments. As explained in above text and Fig. 2, it is expected that the MFM signal at 0.25 T mainly comes from the difference between the FM and non-FM part of the film. The appearance of the magnetic contrast around 4.3 K is in good agreement with the ferromagnetic transition determined by the SQUID magnetization data $M(T)$ [the black filled triangles in Fig. 3(j)]. Furthermore, the temperature dependence of the MFM contrast (RMS values) of the whole scan area [red filled circles in Fig. 3(j)] is in excellent agreement with $M(T)$ after proper scaling, indicating a negligible contribution of non-FM phase below T_C. Thus the change of MFM contrast is mainly due to the sharp rise of saturation magnetization of the FM parts while the induced magnetization of the non-FM is negligibly small. Interestingly, a location

noted by a green box, is qualitatively different from the rest of the imaged area. A fraction of the green box area suddenly becomes brighter at 3.5 K [Fig. 3(f)]. The bright area expands as the temperature decreases. Note that a bright color in MFM corresponds to a local area with a small stray field gradient, i.e. a small local magnetization. Therefore, abrupt increase of MFM signal is equivalent with abrupt reduction of the local magnetization, indicating that an AFM phase formed within the green boxed area. Approximately 5-10% of the non-FM surface shows such AFM-like behavior, demonstrating the majority of non-FM parts are probably in the PM phase. Figure 3(j) shows the temperature-dependence of RMS values of the local area (green squares). The jump at 3.5 K of the green curve corresponds to the sharp change within green box in Fig. 3(f). Note that the anomaly of SQUID magnetization [black curve in fig. 3(j)] at 3.1 K originates from the AFM transition of the $DyScO_3$ substrate,[29] while the MFM image at 3.0 K [Fig. 3(i)] does not show any visible change from the images at higher temperatures. This clearly demonstrates that a uniform stray field background from the $DyScO_3$ substrate does not interfere with MFM measurements.

A representative line profile (upper panel) and a cartoon (lower panel) are shown in Fig. 3(k) to illustrate the magnetic inhomogeneity in the film. Since the average magnetization of the film is $\sim 3\,\mu_B/Eu^{2+}$ (estimated from the magnetization curve), the local magnetization must deviate from this value, i.e. either stronger (FM, $7\,\mu_B/Eu^{2+}$) or weaker (non-FM) magnetization, which is qualitatively consistent with the magnetic inhomogeneity observed by MFM. Consequently, the non-uniform magnetic phases which were directly visualized by MFM provide a physical scenario to explain the missing saturation moment. The origin of the magnetic inhomogeneity is not clear at this moment. One possible mechanism is that a mixed magnetic phase emerges in the thin film because the epitaxial strain lies closely to the phase boundary between AFM-paraelectric and FM-FE. In the light of the structurally nanometer-sized twined phases with nearly degenerate energy suggested by recent theoretical studies, likely there are also multiple or inhomogeneous magnetic ground states in the strained ETO thin films because of strong spin-lattice coupling.[19] Such kind of electronically soft phases provide a new route to engineering giant response (e.g. magnetoelectric coupling) to external stimuli.[32, 33]

In conclusion, our MFM results of ETO/DSO provide direct evidence of local magnetic inhomogeneity in the tensile-strained film, which explains the reduced bulk saturated magnetization in previous studies. The non-FM phases, which are likely PM, reduce the averaged magnetization in bulk measurement. Our real space observation of the mixed phase is consistent with previous findings. The competition between different coupled magnetic-dielectric phases, which can be subtly tuned by epitaxial strain or even electric field, offers plausible prospects to realize 'giant' magnetoelastic or magnetoelectric coupling.[21]

The work at Rutgers was supported by NSF grant DMR-0844807. Work at Argonne was supported by supported by the U. S. Department of Energy under Contract No. DE-AC02-06CH11357.

*corresponding author: wdwu@physics.rutgers.edu

[1] S. W. Cheong and M. Mostovoy, Nature Mater. **6**, 13 (2007).

[2] N. A. Spaldin and M. Fiebig, Science **309**, 391 (2005).

[3] W. Eerenstein, N. D. Mathur, and J. F. Scott, Nature **442**, 759 (2006).

[4] R. Ramesh and N. A. Spaldin, Nature Mater. **6**, 21 (2007).

[5] N. A. Hill, J. Phys. Chem. B **104**, 6694 (2000).

[6] D. G. Schlom, L.-Q. Chen, X. Pan, and A. S. M. A. Zurbuchen, J. Am. Ceram. Soc. **91**, 2429 (2008).

[7] D. G. Schlom, L. Q. Chen, C. B. Eom, K. M. Rabe, S. K. Streiffer, and J. M. Triscone, Annu Rev Mater Res **37**, 589 (2007).

[8] S. Park, P. Ryan, E. Karapetrova, J. W. Kim, J. X. Ma, J. Shi, J. W. Freeland, and W. D. Wu, Appl. Phys. Lett. **95**, 072508 (2009).

[9] J. H. Haeni, P. Irvin, W. Chang, R. Uecker, P. Reiche, Y. L. Li, S. Choudhury, W. Tian, M. E. Hawley, B. Craigo, A. K. Tagantsev, X. Q. Pan, S. K. Streiffer, L. Q. Chen, S. W. Kirchoefer, J. Levy, and D. G. Schlom, Nature **430**, 758 (2004).

[10] K. J. Choi, M. Biegalski, Y. L. Li, A. Sharan, J. Schubert, R. Uecker, P. Reiche, Y. B. Chen, X. Q. Pan, G. V, L. Q. Chen, D. G. Schlom, and C. B. Eom, Science **306**, 1005 (2004).

[11] L. Martin, S. P. Crane, Y. H. Chu, M. B. Holcomb, M. Gajek, M. Huijben, C. H. Yang, N. Balke, and R. Ramesh, J Phys-Condens Mat **20**, 434220 (2008).

[12] J. H. Lee, L. Fang, E. Vlahos, X. Ke, Y. W. Jung, L. F. Kourkoutis, J.-W. Kim, P. J. Ryan, T. Heeg, M. Roeckerath, V. Goian, M. Bernhagen, R. Uecker, P. C. Hammel, K. M. Rabe, S. Kamba, J. Schubert, J. W. Freeland, D. A. Muller, C. J. Fennie, P. Schiffer, V. Gopalan, E. Johnston-Halperin, and D. G. Schlom, Nature **466**, 954 (2010).

[13] C. J. Fennie and K. M. Rabe, Phys. Rev. Lett. **97**, 267602 (2006).

[14] T. Katsufuji and H. Takagi, Phys. Rev. B **64**, 054415 (2001).

[15] J.-W. Kim, P. Thompson, S. Brown, P. S. Normile, J. A. Schlueter, A. Shkabko, A. Weidenkaff, and P. J. Ryan, Phys. Rev. Lett. **110**, 027201 (2013).

[16] M. Allieta, M. Scavini, L. J. Spalek, V. Scagnoli, H. C. Walker, C. Panagopoulos, S. S. Saxena, T. Katsufuji, and C. Mazzoli, Phys. Rev. B **85**, 184107 (2012).

[17] V. Goian, S. Kamba, O. Pacherova, J. Drahokoupil, L. Palatinus, M. Dusek, J. Rohlicek, M. Savinov, F. Laufek, W. Schranz, A. Fuith, M. Kachlik, K. Maca, A. Shkabko, L. Sagarna, A. Weidenkaff, and A. A. Belik, Phys. Rev. B **86**, 054112 (2012).

[18] V. Scagnoli, M. Allieta, H. Walker, M. Scavini, T. Katsufuji, L. Sagarna, O. Zaharko, and C. Mazzoli, Phys. Rev. B **86**, 094432 (2012).

[19] Y. Yang, W. Ren, D. Wang, and L. Bellaiche, Phys. Rev. Lett. **109**, 267602 (2012).

[20] K. Z. Rushchanskii, N. A. Spaldin, and M. Lezaic, Phys. Rev. B **85**, 104109 (2012).

[21] P. J. Ryan, J.-W. Kim, T. Birol, P. Thompson, J.-H. Lee, X. Ke, P. S. Normile, E. Karapetrova, P. Schiffer, S. D. Brown, C. J. Fennie, and D. G. Schlom, Nat. Commun. **4**, 1334 (2013).

[22] B. Velickov, V. Kahlenberg, R. Bertram, and M. Bernhagen, Z Kristallogr **222**, 466 (2007).

[23] M. Schmidbauer, A. Kwasniewski, and J. Schwarzkopf, Acta Crystallogr B **68**, 8 (2012).

[24] M. D. Biegalski, J. H. Haeni, S. Trolier-McKinstry, D. G. Schlom, C. D. Brandle, and A. J. Ven Graitis, J Mater Res **20**, 952 (2005).

[25] S. Park, Y. Horibe, Y. J. Choi, C. L. Zhang, S. W. Cheong, and W. D. Wu, Phys. Rev. B **79**, 180401(R) (2009).

[26] D. Rugar, H. J. Mamin, P. Guethner, S. E. Lambert, J. E. Stern, I. Mcfadyen, and T. Yogi, J. Appl. Phys. **68**, 1169 (1990).

[27] T. R. Albrecht, P. Grutter, D. Horne, and D. Rugar, J. Appl. Phys. **69**, 668 (1991).

[28] W. D. Wu, C. Israel, N. Hur, S. Park, S. W. Cheong, and A. De Lozanne, Nat. Mater. **5**, 881 (2006).

[29] X. Ke, C. Adamo, D. G. Schlom, M. Bernhagen, R. Uecker, and P. Schiffer, Appl. Phys. Lett. **94**, 152503 (2009).

[30] E. Arenholz, A. Schmehl, D. G. Schlom, and G. van der Laan, J. Appl. Phys. **105**, 07E101 (2009).

[31] X. Ke, (private communication).

[32] T. Birol, N. A. Benedek, H. Das, A. L. Wysocki, A. T. Mulder, B. M. Abbett, E. H. Smith, S. Ghosh, and C. J. Fennie, Curr. Opin. Solid. St. M **16**, 227 (2012).

[33] G. C. Milward, M. J. Calderon, and P. B. Littlewood, Nature **433**, 607 (2005).